THE JOURNAL OF BIOLOGICAL CHEMISTRY VOL. 282, NO. 31, pp. 22865–22878, August 3, 2007

Effects of the Isoform-specific Characteristics of ATF6α and ATF6β on Endoplasmic Reticulum Stress Response Gene Expression and Cell Viability*

Received for publication, February 8, 2007, and in revised form, May 22, 2007 Published, JBC Papers in Press, May 23, 2007, DOI 10.1074/jbc.M701213200

Donna J. Thuerauf, Marie Marcinko, Peter J. Belmont[1], and Christopher C. Glembotski[2]

From the San Diego State University Heart Institute and Department of Biology, San Diego State University, San Diego, California 92182

The endoplasmic reticulum (ER)-transmembrane proteins, ATF6α and ATF6β, are cleaved during the ER stress response (ERSR). The resulting N-terminal fragments (N-ATF6α and N-ATF6β) have conserved DNA-binding domains and divergent transcriptional activation domains. N-ATF6α and N-ATF6β translocate to the nucleus, bind to specific regulatory elements, and influence expression of ERSR genes, such as glucose-regulated protein 78 (GRP78), that contribute to resolving the ERSR, thus, enhancing cell viability. We previously showed that N-ATF6α is a rapidly degraded, strong transcriptional activator, whereas β is a slowly degraded, weak activator. In this study we explored the molecular basis and functional impact of these isoform-specific characteristics in HeLa cells. Mutants in the transcriptional activation domain or DNA-binding domain of N-ATF6α exhibited loss of function and increased expression, the latter of which suggested decreased rates of degradation. Fusing N-ATF6α to the mutant estrogen receptor generated N-ATF6α-MER, which, without tamoxifen exhibited loss-of-function and high expression, but in the presence of tamoxifen N-ATF6α-MER exhibited gain-of-function and low expression. N-ATF6β conferred loss-of-function and high expression to N-ATF6α, suggesting that ATF6β is an endogenous inhibitor of ATF6α. *In vitro* DNA binding experiments showed that recombinant N-ATF6β inhibited the binding of recombinant N-ATF6α to an ERSR element from the GRP78 promoter. Moreover, siRNA-mediated knock-down of endogenous ATF6β increased GRP78 promoter activity and GRP78 gene expression, as well as augmenting cell viability. Thus, the relative levels of ATF6α and -β, may contribute to regulating the strength and duration of ATF6-dependent ERSR gene induction and cell viability.

Stresses that alter the rough ER[3] environment can impair folding of proteins synthesized by this organelle (1–4). Numerous proteins induced under such conditions are targeted to the ER, where they aid in nascent protein folding and thus, counteract the stress; this ER-initiated signaling process is known as the ER stress response (ERSR). ERSR elements (ERSEs) are located in the regulatory regions of many ERSR genes. One of the transcription factors that mediates ERSR gene induction via ERSEs is ATF6α, a 670-aa ER trans-membrane protein (5, 6) (Fig. 1*A*, ATF6α). ER stress activates the proteolytic cleavage of ~400 aa from the N terminus of ATF6α (N-ATF6α) (7), which translocates to the nucleus and activates numerous ERSR genes (8, 9). The transcriptional activation domain (TAD) of N-ATF6α resides in the N-terminal portion of the protein, whereas the basic leucine zipper (b-Zip) and nuclear localization domains reside in the C terminus (Fig. 1*B*, N-ATF6α) (8, 10). N-ATF6α can bind directly to ATF6 binding sites (9), or it can combine with several other proteins to form a complex that binds to ERSEs and augments the induction of numerous ERSGs, such as the ER chaperone, glucose-regulated protein 78 kDa (GRP78) (8, 9, 11–13). N-ATF6α exhibits potent transcriptional activity, however, it is susceptible to proteasome-mediated degradation, and mutations in the TAD that reduce N-ATF6α transcriptional activity decrease degradation (14). Several other potent transcription factors that exert rapid, transient effects exhibit similar coupling of transcriptional activation and degradation (15), including the virally encoded protein, VP16 (16). An 8-aa domain in VP16, called VN8, confers strong transcriptional activity and susceptibility to degradation, and mutations in VN8 that reduce VP16 activity decrease degradation (17, 18). The TAD of ATF6α possesses a VN8-like sequence, and mutating it in ways known to decrease VP16 activity decrease ATF6α activity and degradation (14). To the best of our knowledge, the VN8 domain has not been found in any other mammalian transcription factor, including a second isoform of ATF6, ATF6β.

Like ATF6α, ATF6β is an ER-transmembrane protein (Fig. 1*A*, ATF6β), and during ER stress proteolysis generates an N-terminal fragment of ~400 aa (19). N-ATF6α and N-ATF6β possess highly conserved b-Zip domains, which allow them to bind to ERSEs as homo- or heterodimers (20); however, the N-terminal regions are divergent. For example, the region of

* This work was supported in part by National Institutes of Health Grants HL75573 and NS025037 (to C. C. G.). The costs of publication of this article were defrayed in part by the payment of page charges. This article must therefore be hereby marked "*advertisement*" in accordance with 18 U.S.C. Section 1734 solely to indicate this fact.

[1] Funded by a San Diego State University Heart Institute/Rees-Sealy Research Foundation graduate fellowship, and a graduate fellowship from the San Diego Chapter of the Achievment Rewards for College Scientists Foundation.

[2] To whom correspondence should be addressed: Dept. of Biology, San Diego State University, 5300 Campanile Drive, San Diego CA 92182. Tel.: 619-594-2959; Fax: 619-594-5676; E-mail: cglembotski@sciences.sdsu.edu.

[3] The abbreviations used are: ER, endoplasmic reticulum; ERSR, ER stress response; aa, amino acid(s); N-ATF6α, N-terminal ATF6α; TAD, transcriptional activation domain; b-Zip, basic leucine zipper; GRP78, glucose-regulated protein 78; MER, mutant estrogen receptor; ANOVA, analysis of variance; CMV, cytomegalovirus; DBD, DNA-binding domain; siRNA, small interfering RNA; EMSA, electrophoretic mobility shift assay; ERSE, ERSR element; CHX, cycloheximide; TM, tunicamycin; STAT, signal transducers and activators of transcription; XBP1, X-box-binding protein 1.

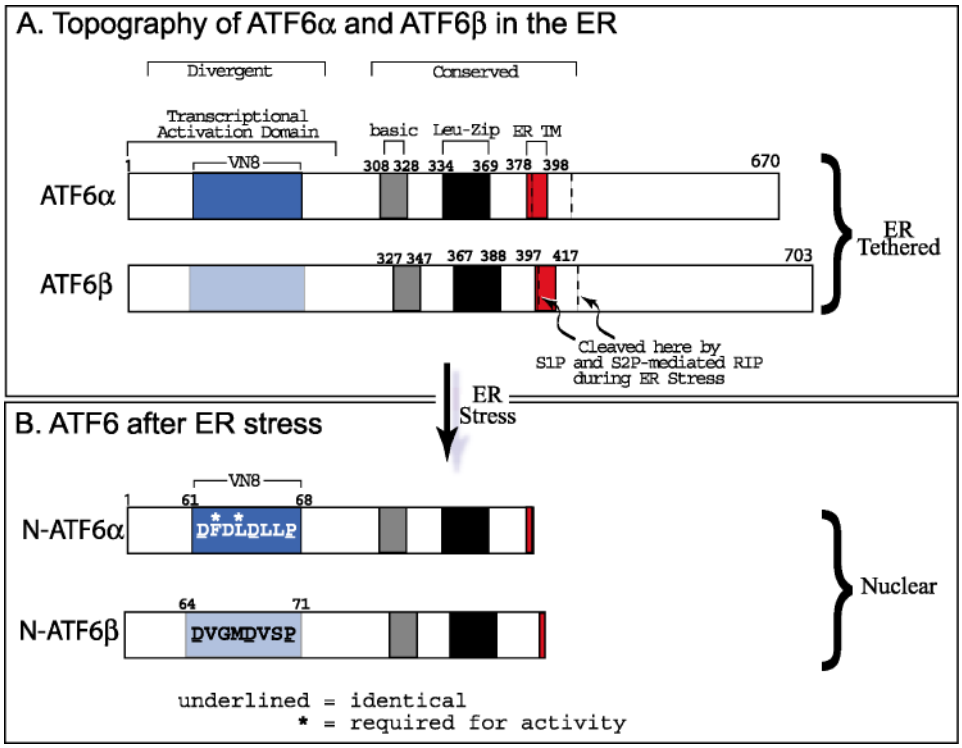

FIGURE 1. **Diagram of ATF6α and ATF6β.** *A*, topography of ATF6α and -β in the ER. The *diagram* depicts the topography of various domains of interest in full-length ATF6α-(1–673) and β-(1–703), which have been mapped in previous studies (6, 14, 19, 20, 22). These forms of ATF6α and -β, which are localized to the ER, exhibit conserved sequences in the basic, leucine-zipper (*Leu-Zip*) and ER transmembrane (*ER TM*) domains, but divergent sequences in the N-terminal transcriptional activation domains. ER stress stimulates the regulated intramembranous proteolysis (*RIP*) of both ATF6α and -β near and in the ER-transmembrane domains by the Golgi-associated proteases, S1P and S2P (7). *B*, ATF6 after ER stress: The *diagram* depicts the N-terminal, "active" forms of ATF6α and -β, which are called N-ATF6α and N-ATF6β in this study. Also shown are the eight amino acids comprising the VN8 region of ATF6α, which is required for optimal transcriptional activity and degradation (14). The homologous region between residues 64 and 71 of ATF6β is shown to emphasize the lack of the Phe and Leu that are required for activity in ATF6α.

N-ATF6β corresponding to the VN8 of N-ATF6α differs in 5 of 8 aa in ways predicted from studies with VP16 to diminish transcriptional activity (21) (Fig. 1*B*, N-ATF6β). In support of this prediction were findings that ectopically expressed N-ATF6β is a poor ERSR gene inducer (6) that exhibits much greater stability than N-ATF6α (14). Accordingly, although they can bind to the same regulatory elements, N-ATF6α and -β exhibit isoform-specific transcriptional activation and stability characteristics. Thus, N-ATF6α and -β might function in a combinatorial fashion to fine-tune the strength of ERSR gene activation.

In the present study, we examined the molecular mechanism and function of the isoform-specific characteristics of N-ATF6α and -β, addressing the following hypotheses: 1) the isoform-specific characteristics of N-ATF6α and -β are conferred by their divergent N-terminal TADs; 2) N-ATF6α-mediated transcriptional activation and rapid degradation are coordinated processes, and 3) the relative levels of N-ATF6α and -β impact ERSR gene induction and cell viability in ways consistent with roles of N-ATF6β as a transcriptional repressor of N-ATF6α.

EXPERIMENTAL PROCEDURES

Methods

Replicates and Statistical Analysis—Unless otherwise stated in the legends or figures, each treatment was performed on three identical cultures, and each experiment was repeated at least three times. Representative experiments are shown. Statistical analyses were performed using a one-way ANOVA followed by the Student-Newman-Keul post-hoc analysis. *, #, or § = $p < 0.05$; **, ##, §§, or ⊕⊕ = $p < 0.01$.

Cell Culture—HeLa Cells were maintained in Dulbecco's modified Eagle's medium containing 10% fetal calf serum. For transfection experiments, HeLa cells were resuspended at 5–9 × 10^6 cells per 400 μl of cold Dulbecco's phosphate-buffered saline and electroporated in a 0.4-cm gap electroporation cuvette at 250 V and 950 microfarads using a GenePulser II Electroporator (Bio-Rad). The cells were then plated at a density of 0.5 × 10^6 per 24-mm well for experiments involving luciferase and β-galactosidase enzyme assays, or 1.5 × 10^6 per 35-mm well for experiments involving immunoblotting. Reporter assays and immunoblotting were carried out as previously described (22).

Plasmids

CMV-Galactosidase—CMV-β-galactosidase, which codes for a β-galactosidase reporter driven by the CMV promoter, was used to normalize for transfection efficiency.

N-ATF6β-VN8 Mutations—Mutations were introduced into 3× FLAG-ATF6β-(1–392) to mimic the VN8 region of ATF6α. Accordingly, the following changes were introduced into ATF6β-VN8-M1: V65F, G66D, and M67L; whereas the following changes were introduced into ATF6β-VN8-M2: V65F, G66D, M67L, V69L, and S70L. ATF6β-VN8-M1 and ATF6β-VN8-M2 were created by PCR, using QuikChange from Stratagene and the relevant primers required to introduce the desired amino acid substitutions.

N-ATF6α and N-ATF6β Chimeras—Constructs encoding chimeric proteins composed of various portions of N-ATF6α and -β were designed by aligning the sequences of N-ATF6α and -β and selecting homologous regions for domain swapping studies. Appropriate PCR fragments were generated from 3× FLAG-N-ATF6α and -β, so that an XhoI restriction site was introduced at the ATF6α and -β junction in each chimera. The amino acid sequence used to name each chimera refers to the original, full-length sequence of either ATF6α and -β. The constructs generated are: ATF6α-(1–114)/ATF6β-(116–392), ATF6α-(1–180)/ATF6β-(191–392), and ATF6α-(1–302)/ATF6β-(322–392), which are named *constructs 3*, *4*, and *5*, respectively, in Fig. 3*A*.

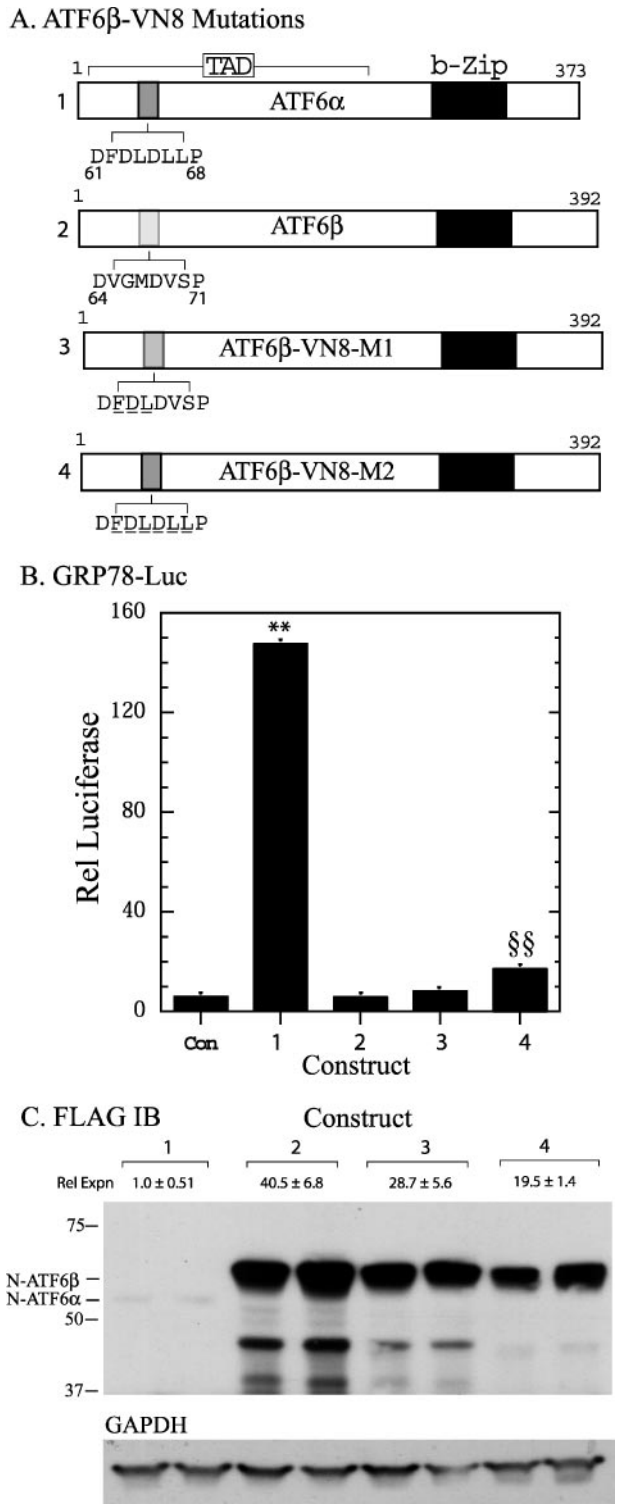

FIGURE 2. **Effect of VN8 mutations on the activity and expression of N-ATF6β.** *A*, *diagram*: shown are the four constructs used in this experiment. *Constructs 1* and *2* are native N-ATF6α and -β, respectively. The mutations prepared in the N-terminal region of N-ATF6β are *underlined* in the *diagrams* of *constructs 3* and *4*. In N-ATF6β-VN8-M1 (*construct 3*), residues 65–67 of N-ATF6β were mutated as follows: V65F, G66D, and M67L. In ATF6β-VN8-M2 (*construct 4*), residues 69 and 70 of N-ATF6β-VN8-M1 were mutated as follows: V69L and S70L. *B*, GRP78 promoter activity: HeLa cells were transfected with either an empty vector control (*Con*), or with one of the four constructs shown in *A*. Cells were co-transfected with either pGL2P, or GRP78-luciferase, and CMV-β-galactosidase, plated, and 48 h later, extracted and analyzed for reporter enzyme activities, as described under "Methods." *Rel Luciferase* is the mean value for GRP78-luciferase/β-galactosidase divided by pGL2P-luciferase/β-galactosidase for each sample ± S.E., $n = 3$ cultures. Values for *Con*, *construct 2* and *3*, are in one group, and ** and §§ = $p < 0.01$ are different from all other values, as determined using ANOVA followed by Newman-Keuls post hoc analysis. *C*, FLAG immunoblot (*IB*): Extracts from the cultures described in *B* were analyzed by SDS-PAGE and immunoblotting for FLAG. *Constructs 1–4* refer to the same constructs shown in *A*. The mean relative expression levels (*i.e.* N-ATF6α or N-ATF6β/GAPDH) ± S.D. are shown at the *top* of each gel.

N-ATF6α and N-ATF6β Gal4 DBD Fusion Proteins—A construct encoding the Gal4 DBD fused to the N terminus of ATF6α-(1–114) (*i.e.* Gal4 DBD-ATF6α-(1–114)) was created by PCR, using 3× FLAG-ATF6α-(1–373) as the template, and the appropriate primers, to create an amplicon with a BamH1 site on the 5′-end, and a termination codon and SacI site on the 3′-end. This PCR product was then cloned into Gal4 DBD (pSG424, GenBank™ accession number X85976). Clones Gal4 DBD-M (L32P) and Gal4 DBD-M (L32P)-ATF6α-(1–114) were generated using QuikChange from Stratagene and the appropriate primers.

N-ATF6α-MER Fusion Protein—A PCR product composed of the nucleotides encoding aa 281–599 of the mouse mutated (G525R) estrogen receptor (MER, a gift from Dr. Michael Reth, Max-Plank-Institute, Freiburg, Germany) was cloned into the NotI/EcoR1 site of pCDNA3.1-3× FLAG vector to create 3× FLAG-MER. Subsequently, a PCR product of N-ATF6α was generated, which introduced a NotI site and removed the termination site after aa 373, was cloned into the XhoI/NotI site of 3× FLAG-MER to create 3× FLAG-N-ATF6α-MER.

3× HA-ATF6β—3× HA-ATF6β was generated by subcloning N-ATF6β from 3× FLAG-N-ATF6β into pCDNA3.1-3× HA, which has been described elsewhere (22).

GRP78-Promoter-luc—Reporter constructs encoding the GRP78 promoter from −284 to +7 or −284 to +221 driving luciferase have been described elsewhere (23).

Small Interfering RNAs

The use of small interfering (si) RNA targeted against human ATF6α and -β has been described elsewhere (22). Briefly, HeLa cells were plated on 6-well plates at ~400 K cells per well, then transfected with 50 ng of the relevant dicer siRNAs, using Lipofectamine 2000™. After 24 h, cells were treated with or without tunicamycin (2 μg/ml), and then examined by real-time quantitative PCR (see below), or, before tunicamycin treatment, they were removed from the plate with TripLE (Invitrogen), and re-plated in 96-well plates at ~10 K cells per well in preparation for viability assays. To examine viability, cells in 96-well plates were treated with or without tunicamycin (2 μg/ml) and 2-deoxyglucose (3 mM) in serum-free media for 32 h. Cell viability was then assessed using an MTT Cell Proliferation Kit according to the manufacturer's protocol (Roche Applied Science). Samples were read at 570 nm in a VersaMax microplate reader (Molecular Devices, Downingtown, PA).

Real-time Quantitative PCR

HeLa cells were transfected with the appropriate siRNA, as described above, then after treatments, they were lysed and RNA was extracted using an RNeasy kit (Qiagen). cDNA was generated by reverse transcription using a Superscript III kit (Invitrogen).

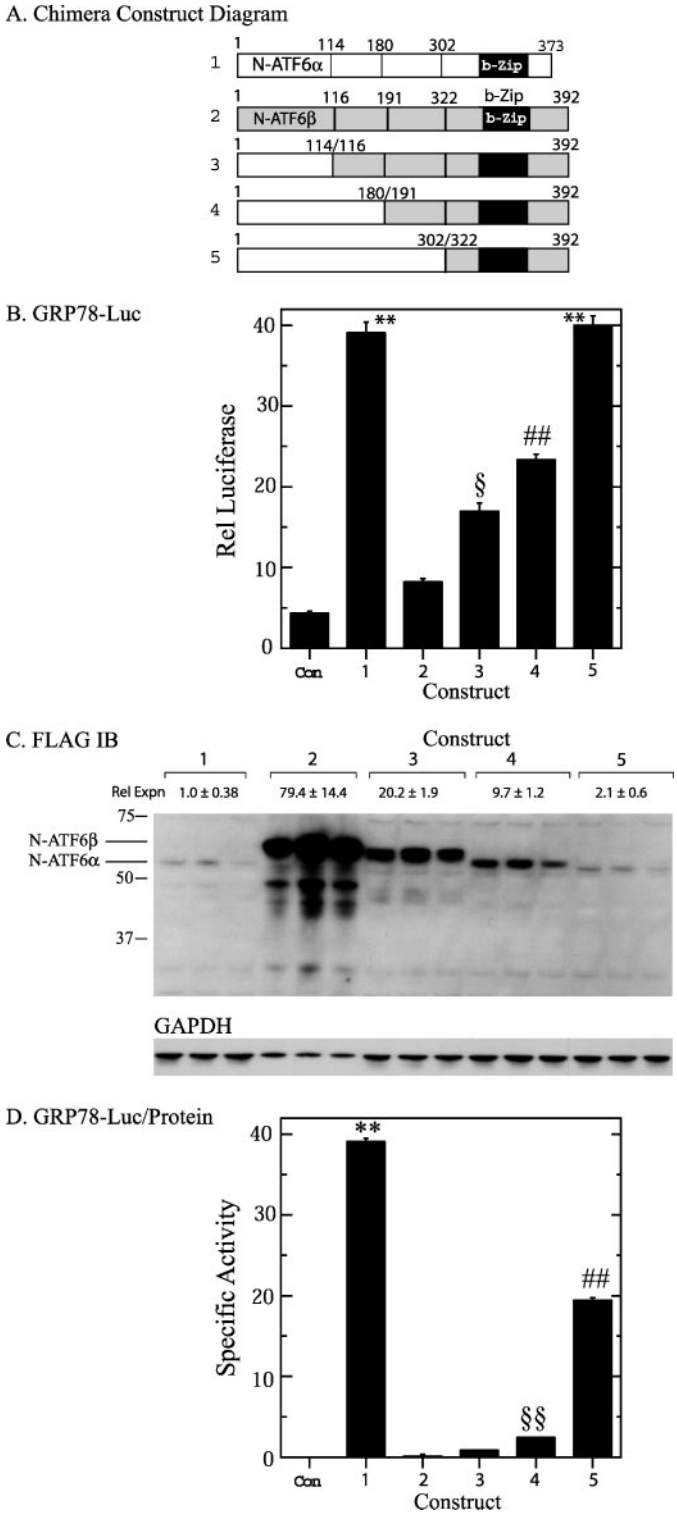

FIGURE 3. **Effect of N-ATF6α and -β domain-swap mutations on transcriptional activity and expression levels.** *A*, chimera construct diagram: Constructs that encode chimeras of N-ATF6α and -β used in this experiment are shown. *Constructs 1* and *2* are native N-ATF6α and N-ATF6β, respectively. In the diagrams of *constructs 3–5*, the *white boxes* represent sequences from ATF6α and *gray boxes* represent sequences from ATF6β. The locations of the boundaries from each ATF6 isoform are shown; for example, *construct 3* is composed of ATF6α-(1–114) fused to ATF6β-(116–392). The boundary amino acids were selected based on sequence homology. *B*, GRP78 promoter activity: HeLa cells were co-transfected with either an empty vector control (*Con*), or the ATF6 expression constructs shown, and GRP78-luciferase or pGL2P and CMV-β-galactosidase, as in Fig. 2. After 48 h in culture, extracts were assayed for reporter enzyme activities, as described under "Methods." Mean Rel Luciferase ± S.E., $n = 3$ cultures is shown. Values for *Con* and *construct 2* are in one group, §, $p < 0.05$ and **, $p < 0.01$ are different from all other values, as determined using ANOVA followed by Newman-Keuls post hoc analysis. *C*, FLAG immunoblot (*IB*): extracts from the cultures described in *B* were analyzed by SDS-PAGE and immunoblotting for FLAG. *Constructs 1–5* refer to the same constructs shown in *A*. The mean relative expression levels of each expression protein ± S.E. are shown at the *top* of each gel. *D*, GRP78 promoter activity normalized to protein levels: The mean Rel Luciferase values from *B* were divided by the mean expression levels of each protein from *C*, to generate the specific activity. Values for *Con* and *constructs 2* and *3* are in one group, ##, §§, and ** = $p < 0.01$ are different from all other values, as determined using ANOVA followed by Newman-Keuls post hoc analysis.

Real-time quantitative PCR was performed on cDNA using the Quanti-Tect SYBR Green PCR kit (Qiagen) on an ABI Prism 7000 (Applied Biosystems, Foster City, CA). The relative abundance of GRP78 RNA was calculated using the $\Delta\Delta C_t$ method, as previously described (24). Primers (see below) were designed using primer express version 2.0 (Applied Biosystems). All primers were determined to be 90% to 110% efficient, and all exhibited only one dissociation peak as follows: GRP78: (+) CCACCTCAGTCTCCCAGCTAA; (−) GCCGAGCATGGTGGTAACA; ATF6α: (+) CACAGCTCCCTAATCACGTGG; (−) ACTGGGCTATTCGCTGAAGG; ATF6β: (+) CAGCCATCAGCCACAACAAG; (−) GGCATCACCAGGGACATCTT; and glyceraldehyde-3-phosphate dehydrogenase: (+) GCCACATCGCTCAGACACC; (−) CAAATCCGTTGACTCCGACC.

Electrophoretic Mobility Shift Assays

Electrophoretic mobility shift assays (EMSAs) were carried out essentially as previously described (25). Double-stranded synthetic oligonucleotides were used as ^{32}P-labeled probes or competitors, as described in the figure legends. The GRP78 ERSE-1 sequence was: CCGGGAGGGCCTTCACCAATCGGCGGCCTCCACGACGGGGCTGGC (underlined nucleotides are a consensus ERSE), and the GRP78 ERSE1 MM sequence was CCGGGAGGGCCTTCAgactaCGGCGGCCTgatgtACGGGGCTGGC (mutated nucleotides indicated by lowercase). Nuclear extracts, which provide the source of other proteins (*e.g.* NF-Y, YY1, and TFII-I) needed for ATF6 binding to ERSEs, were prepared as previously described (25). Binding reactions were carried out in a solution composed of 20 mM HEPES (pH 7.9), 10% glycerol, 1 mM $MgCl_2$, 1 mM 2-mercaptoethanol, 0.1% Tween 20, 0.2 μg of poly(dI-dC), 6 μg of HeLa nuclear extract, 2 μl of *in vitro* translated ATF6α-(1–373), ATF6α-(115–373), or ATF6β-(1–392), prepared as previously described (10), and 10,000 cpm of ^{32}P-labeled probe. Reactions were incubated at room temperature for 20 min, and then fractionated on a 5% polyacrylamide gel at 200 V for 150 min in 0.5× TBE buffer (45 mM Tris borate, 1 mM EDTA). For supershift EMSAs, 1 μl of anti-ATF6α (Santa Cruz Biotechnology, sc-22799), 1 μl of anti-ATF6β (Santa Cruz Biotechnology, sc-30596), or 1 μl of non-immune mouse antisera was added 15 min prior to probe addition. For oligonucleotide specificity assessment, 250-fold excess of unlabeled double-stranded oligonucleotide was added 15 min prior to addition of probe.

RESULTS

Isoform-specific Characteristics of N-ATF6α and -β Are Conferred by Their Divergent N-terminal TADs—Because we previously showed the importance of the VN8 sequence for

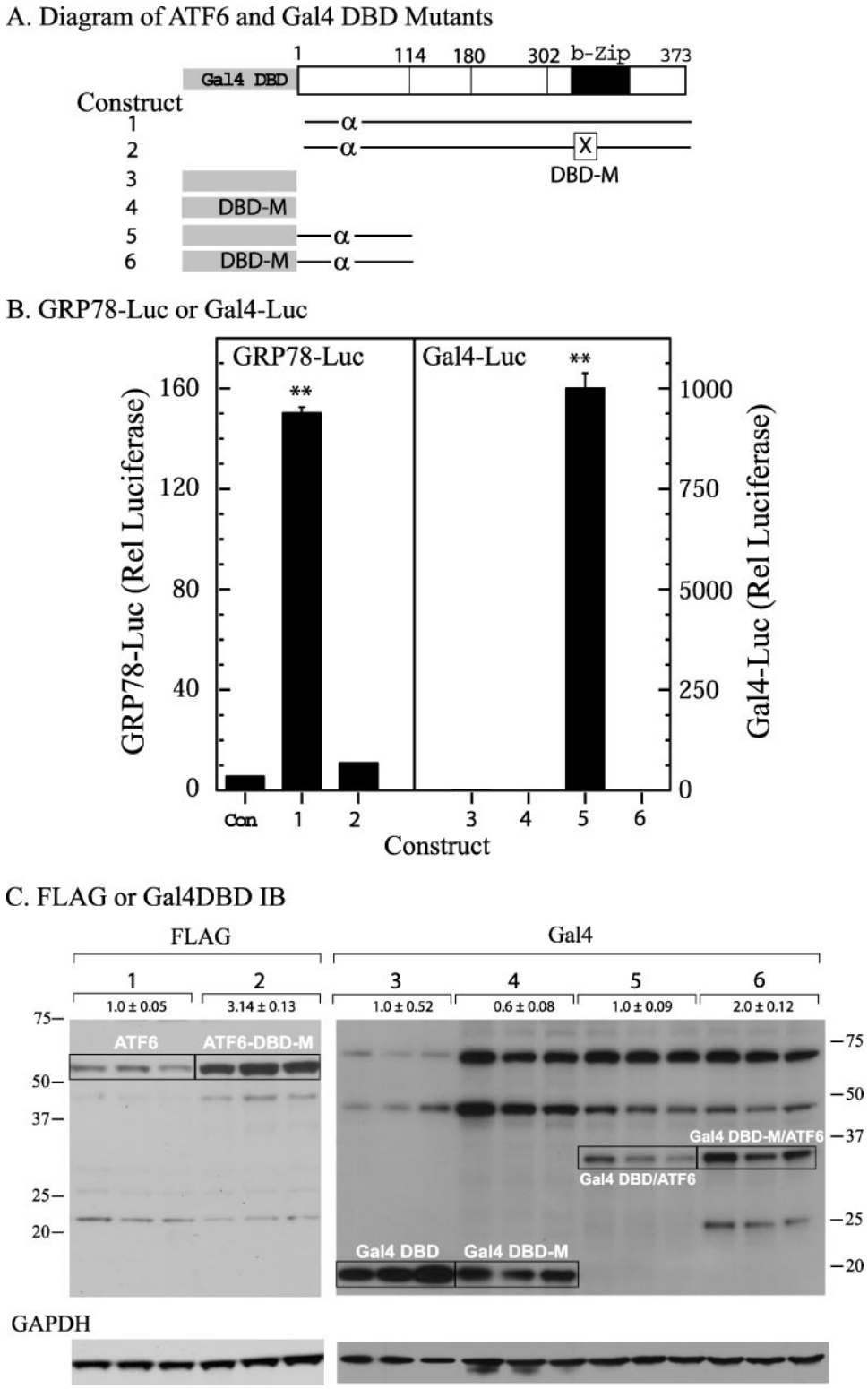

FIGURE 4. **Effect of DNA binding mutants on N-ATF6α and ATF6α-(1–114)/Gal4 DBD.** *A*, *diagram* of ATF6 and Gal4 DBD mutants. *Construct 1* is native N-ATF6α, and *construct 2* is N-ATF6α with the following mutations in the DNA-binding domain: K315T, N315A, and R315A, as previously described (9). *Construct 3* encodes the native Gal4 DBD, whereas *construct 4* encodes Gal4 DBD-M with a DNA-binding domain mutation, L32P. *Construct 5* encodes native Gal4 DBD fused to the N terminus of ATF6α-(1–114), whereas *construct 6* encodes the same Gal 4 DBD-M fused to the N terminus of ATF6α-(1–114). *B*, GRP78 luciferase or Gal4 luciferase: HeLa cells were transfected with the constructs shown (*Con* = empty vector), and either GRP78-luciferase, or Gal4-luciferase, and after 48 h in culture, extracts were assayed for reporter enzyme activities, as described under "Methods." *Rel Luciferase* = GRP78-luciferase/β-galactosidase, or Gal4-luciferase/β-galactosidase. Shown are mean Rel Luciferase values ± S.E. ($n = 3$ cultures). In the GRP78-Luc panel, values for Con and *construct 2* are in one group, and in the Gal4-Luc panel, *constructs 3*, *4*, and *6* are in one group. For both panels, **, $p < 0.01$ are different from all other values in that panel, as determined using ANOVA followed by Newman-Keuls post hoc analysis. *C*, FLAG and Gal4 DBD immunoblots (*IB*): extracts from the cultures described in *B* were analyzed by SDS-PAGE and immunoblotting for FLAG or Gal4, as shown. *Constructs 1–6* refer to the same constructs shown in *A*. All *lanes* were loaded with 30 μg of protein, except those for *construct 3*, which were loaded with 3 μg. The mean relative expression levels ± S.E. are shown at the *top* of each gel.

the transcriptional activity and rapid degradation of ATF6α (22), we assessed whether the lack of a VN8 sequence in ATF6β is responsible for its low transcriptional activity and high stability. Upon sequence alignment of N-ATF6α and -β, we found that residues 64–71 of β correspond to residues 61–68 of α, the VN8-like region (Fig. 1*B*). Accordingly, residues 64–67 of N-ATF6β (*i.e.* ATF6β-(1–392)) were mutated to the same residues found in the VN8-like region of ATF6α, which possess the Phe and Leu known to be required for optimal activity (Fig. 2*A*, *construct 3*, ATF6β-VN8-M1). We also prepared a mutation that converted the entire 64–71 region N-ATF6β to be identical to the VN8 in ATF6α (Fig. 2*A*, *construct 4*, ATF6β-VN8-M2). The abilities of native N-ATF6β or the VN8 mutations to activate the promoter of the prototypical ERSR gene, GRP78, in HeLa cells were compared with N-ATF6α (*i.e.* ATF6α-(1–373)). As previously seen (22), N-ATF6α exerted strong GRP78 promoter activation, whereas native N-ATF6β exhibited weak effects (Fig. 2*B*, *constructs 1 versus 2*). Among the ATF6β VN8 mutations, only ATF6β-VN8-M2 exhibited detectible GRP78 promoter activation, although it amounted to only ~8% of N-ATF6α (Fig. 2*B*, *construct 4*). Previous studies showed that the relative levels of ectopically expressed ATF6α and -β are proportional to their half-lives (22). N-ATF6α was expressed in very low quantities (Fig. 2*C*, *construct 1*), consistent with its known short half-life, whereas all forms of N-ATF6β were expressed at much higher levels (Fig. 2*C*, *constructs 2–4*), suggesting that they exhibited relatively long half-lives, as previously shown for native N-ATF6β (22). Quantification demonstrated that N-ATF6β, N-ATF6β-VN8-M1, and N-ATF6β-VN8-M2 were expressed at ~40-, 29-, and 20-fold higher levels than N-ATF6α, respectively (Fig. 2*C*). Thus, although their expression levels and apparent half-lives decreased in coordination with the minor increases in activity, it was apparent that the low transcriptional activity and high stability of N-ATF6β were not due entirely to the lack of a consensus VN8 sequence, but that larger portions of ATF6β must be required to confer these isoform-specific characteristics.

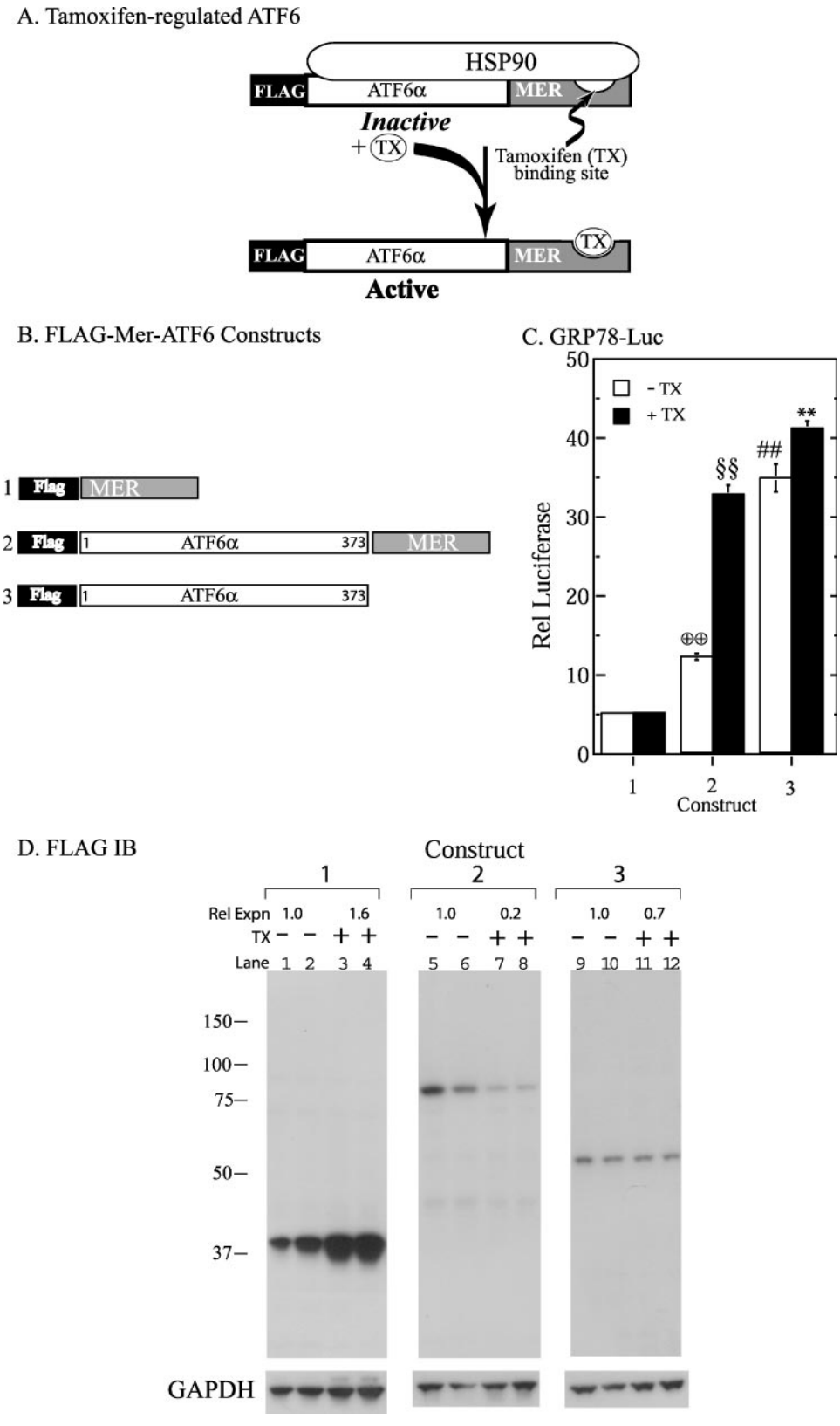

To examine the effects of mutating larger portions of ATF6α and -β, a series of domain-swap mutations were generated where the N terminus of N-ATF6β was replaced with progressively larger portions of the corresponding sequences from N-ATF6α (Fig. 3*A*). As expected, native N-ATF6α was a strong activator of the GRP78 promoter, whereas native N-ATF6β was much weaker (Fig. 3*B*, *constructs 1 versus 2*). However, when the N-terminal 115 or 190 aa of N-ATF6β were replaced with corresponding sequences from α, transcriptional activity increased progressively (Fig. 3*B*, *constructs 3* and *4*). Finally, when the N-terminal 321 aa of N-ATF6β, representing all but the 71-aa b-Zip domain, were replaced by corresponding sequences from N-ATF6α, GRP78 promoter activity increased to about the same level as that observed using native N-ATF6α (Fig. 3*B*, *construct 5*), suggesting that the b-Zip domains of N-ATF6α and -β were interchangeable. As expected, the level of expression of N-ATF6β was ~80-fold greater than N-ATF6α (Fig. 3*C*, *constructs 1* and *2*); moreover, expression levels of the chimeras declined coordinately as more sequences from N-ATF6α replaced corresponding sequences in β (Fig. 3*C*, *constructs 3–5*), consistent with the hypothesis that the degradation rate of ATF6 coordinates with its transcriptional activity. When GRP78 promoter activity was normalized to the levels of ectopic N-ATF6α or -β protein expression, the only domain-swap mutant exhibiting activity approximating that of native N-ATF6α was *construct 5* (Fig. 3*D*). Accordingly, these data suggested that, although the b-Zip domain of ATF6β can substitute for the b-Zip domain of ATF6α without much loss of function, most of the sequences lying to the N terminus of the b-Zip domain of ATF6α are necessary to confer the full transcriptional activity and rapid degradation characteristic of this ATF6 isoform.

N-ATF6α-mediated Transcriptional Activation and Rapid Degradation Are Coordinated Processes—It is not known whether it is the sequences in the TAD of ATF6α that confer strong transcriptional activation and rapid degradation, or whether rapid degradation is a function of the engagement of ATF6α in a productive transcription complex. If the latter is true, then mutating the basic region of the b-Zip domain to disrupt binding of N-ATF6α to ERSEs should decrease transcriptional activation and decrease degradation. Consistent with this hypothesis was our finding that mutating the basic region of N-ATF6α (Fig. 4*A*, *construct 2*) to disrupt the binding of N-ATF6α to ERSEs (9) resulted in decreased GRP78 promoter activation (Fig. 4*B*, *constructs 1* and *2*) and increased N-ATF6α expression of >3-fold (Fig. 4*C*, *FLAG blot*, *constructs 1* and *2*). To test this hypothesis in a heterologous gene expression system, we used a truncated form of the yeast transcription factor Gal4, Gal4-(1–147), composed of the Gal4 DBD, which does not possess a TAD. The binding of the Gal4 DBD to appropriate DNA sequences was assessed using a luciferase reporter driven by a neutral promoter flanked by tandem repeats of the Gal4 binding element. A mutation known to block the binding of Gal4-(1–147) to the Gal4 binding element (26) was introduced into a construct featuring the TAD of ATF6α without the ATF6 DBD, *i.e.* ATF6α-(1–114), fused to the Gal4 DBD (Fig. 4*A*, *constructs 5* and *6*). As expected, the ATF6α(1–114)/Gal4 DBD fusion protein without the DBD mutation exhibited robust transcriptional activation, compared with the Gal4 DBD alone (Fig. 4*B*, *constructs 3* and *5*); however, the ATF6α(1–114)/Gal4 DBD fusion protein harboring the DBD mutation exhibited no transcriptional activation (Fig. 4*B*, *construct 6*). Moreover, the level of expression of ATF6α/Gal4 DBD-M was ~2-fold greater than that of ATF6α/Gal4 DBD (Fig. 4*C*, *Gal4 blot*, *constructs 5* and *6*), whereas the level of expression of Gal4 DBD-M was actually somewhat lower than that of Gal4 DBD (Fig. 4*C*, *Gal4 blot*, *constructs 3* and *4*). These results are consistent with the hypothesis that rapid degradation of N-ATF6α requires its engagement in transcriptional activation.

To examine the relationship between transcriptional engagement and ATF6 degradation in a different model system, we designed a method for conditionally activating N-ATF6α in a ligand-dependent manner. For this purpose, we generated a construct encoding N-ATF6α fused to a fragment of the MER, which has no TAD or DBD, but features a tamoxifen-ligand-binding domain replacing the estrogen-binding domain. By analogy to the way MER affects other proteins to which is has been fused (27), we reasoned that, in the absence of tamoxifen, the MER would attract other cellular components, *e.g.* HSP90, which would block functional domains of ATF6, but that, upon tamoxifen binding, release of HSP90, among others, would reveal functional domains and allow full engagement of ATF6 in transcription (Fig. 5*A*). Accordingly, constructs encoding FLAG-MER or FLAG-N-ATF6α-MER, where MER is fused to the C terminus of FLAG-N-ATF6α, were prepared (Fig. 5*B*), and the abilities of each to activate the GRP78 promoter were examined. As expected, FLAG-MER exhibited essentially no activity (Fig. 5*C*, *construct 1*), whereas FLAG-N-ATF6α exhibited high activity that was affected very little by tamoxifen (Fig. 5*C*, *construct 3*). In contrast, FLAG-N-ATF6α-MER exhibited

FIGURE 5. **Effect of tamoxifen on ATF6α-MER chimera.** *A*, *diagram* of MER mechanism of action: the *diagram* (36) depicts the putative mechanism of action of ATF6α fused to a fragment of the mutant mouse estrogen receptor (*MER*). The construct encodes FLAG-ATF6α with the MER fused to the C terminus. In the absence of ligand (*i.e.* tamoxifen, *TX*), various cellular proteins, *e.g.* HSP90, bind to the MER and mask the function domains of ATF6. Addition of tamoxifen to cultures expressing FLAG-N-ATF6α-MER leads to displacement of HSP90, among others, unmasking of ATF6 functional domains, and activation of ATF6α-dependent transcription. *B*, *diagram* of *constructs*: *constructs 1–3* were generated so they encode FLAG with MER fused to the C terminus of FLAG (*construct 1*), FLAG-N-ATF6α with MER fused to the C terminus of N-ATF6α (*construct 2*), or FLAG-N-ATF6α (*construct 3*). *C*, effect of tamoxifen on GRP78-Luciferase: HeLa cells were transfected with *constructs 1–3* along with GRP78-Luciferase and CMV-β-galactosidase. Cultures were then treated with or without tamoxifen (*TX*) 5 μM, and after 16 h, extracts were prepared and assayed for reporter enzyme activities, as described under "Methods." Mean Rel Luciferase ± S.E., $n = 3$ cultures is shown. The values for *construct 1* with or without TX are in one group, whereas **, ##, §§, or ⊕⊕ = $p < 0.01$ are different from all other values, as determined using ANOVA followed by Newman-Keuls post hoc analysis. *D*, effect of tamoxifen on N-ATF6α-MER expression: HeLa cells were transfected with *constructs 1–3*, treated with or without tamoxifen (*TX*), as described in *B*, and after 48 h, extracts were fractionated by SDS-PAGE followed by FLAG immunoblotting. *Constructs 1–3* refer to the same constructs shown in *B*. The mean relative expression levels ± S.D. are shown at the *top* of each gel.

little activity in the absence of tamoxifen, but, upon tamoxifen addition, activity increased 3-fold, nearly equal to that of FLAG-N-ATF6α (Fig. 5*C*, *construct 2*). The protein levels of FLAG-MER were relatively high in the absence of tamoxifen (Fig. 5*D*, *lanes 1* and *2*), and actually increased by 1.6-fold in the presence of tamoxifen (Fig. 5*D*, *lanes 3* and *4*), which was somewhat expected, because tamoxifen stabilizes MER. The levels of FLAG-N-ATF6α were low and unchanged by tamoxifen (Fig. 5*D*, *lanes 9–12*). However, the levels of FLAG-N-ATF6α-MER were decreased by ~5-fold in tamoxifen-treated cells (Fig. 5*D*, *lanes 5–8*), suggesting coordination of tamoxifen-activated transcription and rapid degradation of FLAG-ATF6α-MER.

Relative Levels of N-ATF6α and -β Impact ERSR Gene Induction and Cell Viability in Ways Consistent with Roles of N-ATF6β as a Transcriptional Repressor of N-ATF6α—The ATF6α loss-of-function mutations in this and previous studies exhibit decreases in degradation. We previously showed that N-ATF6β mimicked ATF6α loss-of-function mutations in terms of inhibiting N-ATF6α-mediated transcription (22), but its effect on ATF6α expression level and degradation is not known. Accordingly, a construct encoding FLAG-N-ATF6α was used to distinguish it from HA-N-ATF6β on immunoblots, and the ratios of ectopically expressed FLAG-N-ATF6α and HA-N-ATF6β were varied by transfecting HeLa cells with different amounts of the appropriate plasmids.

In the first series of experiments, the level of FLAG-N-ATF6α-encoding plasmid was held constant, while the level of the HA-N-ATF6β-encoding plasmid was varied. As expected, GRP78 promoter activation by FLAG-N-ATF6α was inhibited as the level of HA-N-ATF6β was increased (Fig. 6*A*, *transfections 1–3*). FLAG and HA immunoblots showed that the quantity of HA-N-ATF6β increased as a function of increased plasmid, as expected (Fig. 6*B*, HA-ATF6β); interestingly, the levels of FLAG-N-ATF6α also increased, even though each culture had been transfected with the same quantity of the FLAG-N-ATF6α plasmid (Fig. 6*B*, FLAG-ATF6α). These results suggested that HA-N-ATF6β not only inhibited the ability of FLAG-N-ATF6α to activate the GRP78 promoter, but also increased its half-life. We examined degradation of FLAG-N-ATF6α using cycloheximide (CHX) to inhibit new protein synthesis, as previously described (28). The apparent degradation of FLAG-N-ATF6α was extremely rapid when no HA-N-ATF6β was co-expressed. Within 9 min of CHX addition, only 12% of the FLAG-N-ATF6α originally present remained (Fig. 6*C*, *transfection 1*, *Blot A*, *versus transfection 1*, *Blot B*). In contrast, the degradation rate of FLAG-N-ATF6α was reduced in the presence of HA-N-ATF6β; moreover, as the level of HA-N-ATF6β was increased, degradation rate of FLAG-N-ATF6α decreased. For example, at intermediate or high levels of HA-FLAG-N-ATF6β, 66 and 82% of the original FLAG-N-ATF6α remained after 9 min of CHX treatment (Fig. 6*C*, *transfections 2* and *3*, *Blot A versus Blot B*).

In the second series of experiments, the FLAG-N-ATF6α-encoding plasmid was varied, while the HA-N-ATF6β-encoding plasmid was held constant. As expected, HA-N-ATF6β alone conferred very little GRP78 promoter activation (Fig. 6*D*, *transfection 4*), whereas, increasing the levels of FLAG-N-ATF6α increased GRP78 promoter activity (Fig. 6*D*, *transfections 5* and *6*). FLAG and HA immunoblots showed that the level of FLAG-N-ATF6α increased as more plasmid was transfected, as expected (Fig. 6*E*, FLAG-ATF6α, *transfections 4–6*); however, surprisingly, the levels of HA-N-ATF6β decreased, even though each culture had been transfected with the same quantity of that plasmid (Fig. 6*E*, HA-ATF6β, *transfections 5* and *6*). These results suggested that FLAG-N-ATF6α can increase the degradation rate of HA-N-ATF6β. Consistent with this hypothesis was the finding that, in the absence of FLAG-N-ATF6α, ~58% of the original HA-N-ATF6β was still present following 17 min of CHX treatment (Fig. 6*F*, *transfection 4*, *Blot A versus B*). In contrast, the degradation rate of HA-N-ATF6β was increased in the presence of FLAG-N-ATF6α; moreover, as FLAG-N-ATF6α was increased, the degradation rate of HA-N-ATF6β increased. For example, at intermediate and high levels of FLAG-N-ATF6α, 32 and 26% of the original HA-N-ATF6β was still present 17 min after CHX treatment (Fig. 6*F*, *transfections 5* and *6*, *Blot A versus B*). Taken together, the results of the experiments shown in Fig. 6 indicate that ATF6α and -β can influence each other, such that the isoform-specific transcriptional and degradation characteristics of each are dependent upon their relative levels. This finding is consistent with a mechanism whereby N-ATF6α and -β can regulate ERSR gene expression and cellular function in a combinatorial fashion.

Because ATF6α and -β can both bind to ERSEs (20), EMSAs were performed to assess the abilities of recombinant ATF6α and -β to compete for binding to an ERSE in the GRP78 gene. Incubation of nuclear extract from untreated HeLa cells with a labeled oligonucleotide that replicates ERSE-1 in the GRP78 gene resulted in the formation of complex 1 (Fig. 7*A*, *lane 1*). Formation of complex 1 has previously been shown to be due to binding of other nuclear proteins (*e.g.* NF-Y A, B, and C) to the ERSE in the absence of ATF6 (25). Adding recombinant ATF6α-(1–373) or ATF6β-(1–392) to the nuclear extract resulted in the formation of complexes 3 and 4, respectively, which migrated with relative mobilities consistent with the sizes of each form of ATF6 that was added (Fig. 7*A*, *lanes 2* and *3*). Adding a shortened form of ATF6, ATF6α-(115–373), which should retain ERSE-binding ability, also exhibited a complex, complex 2, the mobility of which was consistent with the size of ATF6α-(115–373) relative to the other forms of ATF6 used in this analysis (Fig. 7*A*, *lane 4*). When an excess of unlabeled wild-type GRP78 ERSE-1 oligonucleotide was added to the incubation, all of the complexes disappeared (Fig. 7*A*, *lanes 5–8*), as expected. However, excess unlabeled mutated GRP78 ERSE-1 was unable to compete for labeled oligonucleotide binding (Fig. 7*A*, *lanes 9–12*). These results demonstrate the dependence of each complex on the presence of the native GRP78 ERSE-1.

To verify the presence of ATF6 isoforms in complexes 2–4, supershift EMSA experiments were carried out. Addition of preimmune antiserum to the nuclear extract did not alter the EMSA profile (Fig. 7*B*, *lanes 1–4*). However, addition of an antiserum specific for ATF6α altered the mobility of com-

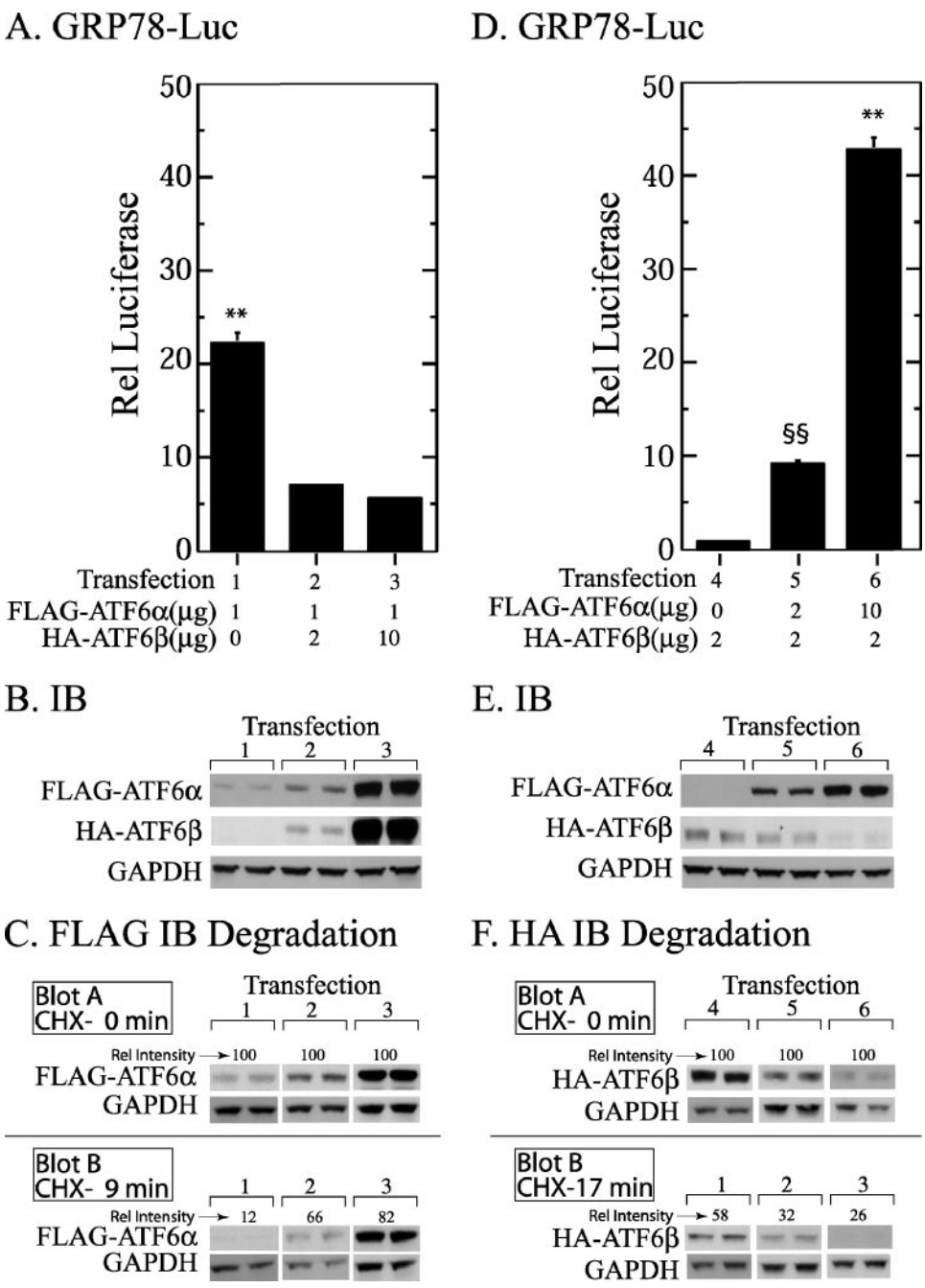

FIGURE 6. **Effect of varying ectopically expressed N-ATF6α, N-ATF6β on GRP78 promoter activation and N-ATF6 expression levels.** *A*, effect of varied N-ATF6β and constant N-ATF6α on GRP78 luciferase: HeLa cells were transfected with GRP78-luciferase, CMV-β-galactosidase, and the amounts of the FLAG-N-ATF6α and HA-N-ATF6β-encoding plasmids shown in *transfections 1–3*. After 48 h, extracts were analyzed for reporter enzyme activities. Mean Rel Luciferase ± S.E., $n = 3$ cultures is shown. **, $p < 0.01$ are different from each other and all other values, as determined using ANOVA followed by Newman-Keuls post hoc analysis. *B*, effect of varied N-ATF6β and constant N-ATF6α on expression levels: extracts from *transfections 1–3*, described in *A*, were fractionated by SDS-PAGE and then examined by FLAG or HA immunoblotting; only the regions of the gel where N-ATF6α or N-ATF6β migrate are shown. *C*, effect of varied N-ATF6β and constant N-ATF6α on degradation: *Blot A*, HeLa cells were transfected as described in *A* and after 48 h in culture, they were extracted and the expression levels of FLAG-N-ATF6α were analyzed by FLAG immunoblotting, as described in *B*. The relative intensity (*Rel Intensity*) refers to the average intensity of FLAG-ATF6α/glyceraldehyde-3-phosphate dehydrogenase (*GAPDH*) in extracts from each transfection. Relative intensities were normalized to 100% for each transfection. *Blot B*, HeLa cells were transfected and treated as described in *Blot A*, except that, before extraction, they were treated for 9 min with 40 μM cycloheximide (*CHX*) to inhibit new protein synthesis, and then extracted followed by SDS-PAGE and FLAG immunoblotting. Nine min was found to be the optimal time of CHX treatment for examining this range of FLAG-ATF6α immunoblot intensities. *Rel intensity* = FLAG-ATF6α/GAPDH in each transfection, divided by the relative intensities for the same transfection before CHX treatment, in *Blot A*. *D*, effect of constant N-ATF6β and varied N-ATF6α on GRP78 luciferase: HeLa cells were transfected with various levels of constructs encoding FLAG-N-ATF6α or HA-N-ATF6β, along with reporter constructs, and then extracts were analyzed for reporter enzyme activity, as described in *A*. Mean Rel Luciferase ± S.E., $n = 3$ cultures is shown. ** and §§ = $p < 0.01$ are different from each other and all other values, as determined using ANOVA followed by Newman-Keuls post hoc analysis. *E*, effect of constant N-ATF6β and varied N-ATF6α on expression levels: extracts from *transfections 4–6*, described in *D*, were fractionated by SDS-PAGE and then examined by FLAG or HA immunoblotting; only the regions of the gel where N-ATF6α or N-ATF6β migrate are shown. *F*, effect of constant N-ATF6β and varied N-ATF6α on N-ATF6β or N-ATF6α degradation: degradation of ectopically expressed HA-N-ATF6β was determined, as described for FLAG-N-ATF6α in *C*. 17 min was found to be the optimal time of CHX treatment for examining this range of HA-ATF6β immunoblot intensities.

plexes 2 and 3, only (Fig. 7*B*, compare *lanes 6* and *8* to *lanes 2* and *4*, respectively), whereas addition of an antiserum specific for ATF6β altered the mobility of complex 4, only (Fig. 7*B*, compare *lane 11* with *lane 3*). These results verify that complex 1 does not contain either form of ATF6, whereas complexes 2–4 contain ATF6α-(115–373), ATF6α-(1–373), and ATF6β-(1–392), respectively.

Additional EMSAs were performed to determine the effects of ATF6α and ATF6β together on complex formation. Addition of ATF6α-(1–373) and ATF6β-(1–392) resulted in a decrease in the intensities of complexes 3 and 4 (Fig. 7*C*, compare *lanes 2* and *3* to *lane 4*). Moreover, adding ATF6α-(115–373) and ATF6β-(1–392) demonstrated a decrease in the intensities of complexes 2 and 4 (Fig. 7*C*, compare *lanes 7* to *lanes 5* and *6*). Taken together, the results of the EMSA studies shown in Fig. 7 support the hypothesis that ATF6α and -β compete for binding to the canonical ERSE-1 in the GRP78 gene.

To examine the cellular effects of altering the relative levels of endogenous ATF6α and -β, we used an siRNA approach that was previously shown by immunoblotting to selectively reduce the quantity of each ATF6 isoform in HeLa cells (22). The selectivity of the siRNA reagents was verified here by quantitative reverse transcription-PCR assessment of ATF6α and -β mRNA in extracts from cells treated with siRNA targeted to green fluorescent protein (control), ATF6α, ATF6β, or another ERSR gene that is not the focus of this study, XBP1. Validating the specificity of the siRNAs was the finding that the ATF6α-targeted siRNA reagent decreased the level of ATF6α and not ATF6β or XBP1 mRNA (Fig. 8*A*), whereas the ATF6β-targeted siRNA decreased the level of ATF6β and not ATF6α or XBP1 mRNA (Fig. 8*B*). Knocking down ATF6α decreased basal and tunicamycin (TM)-stimulated

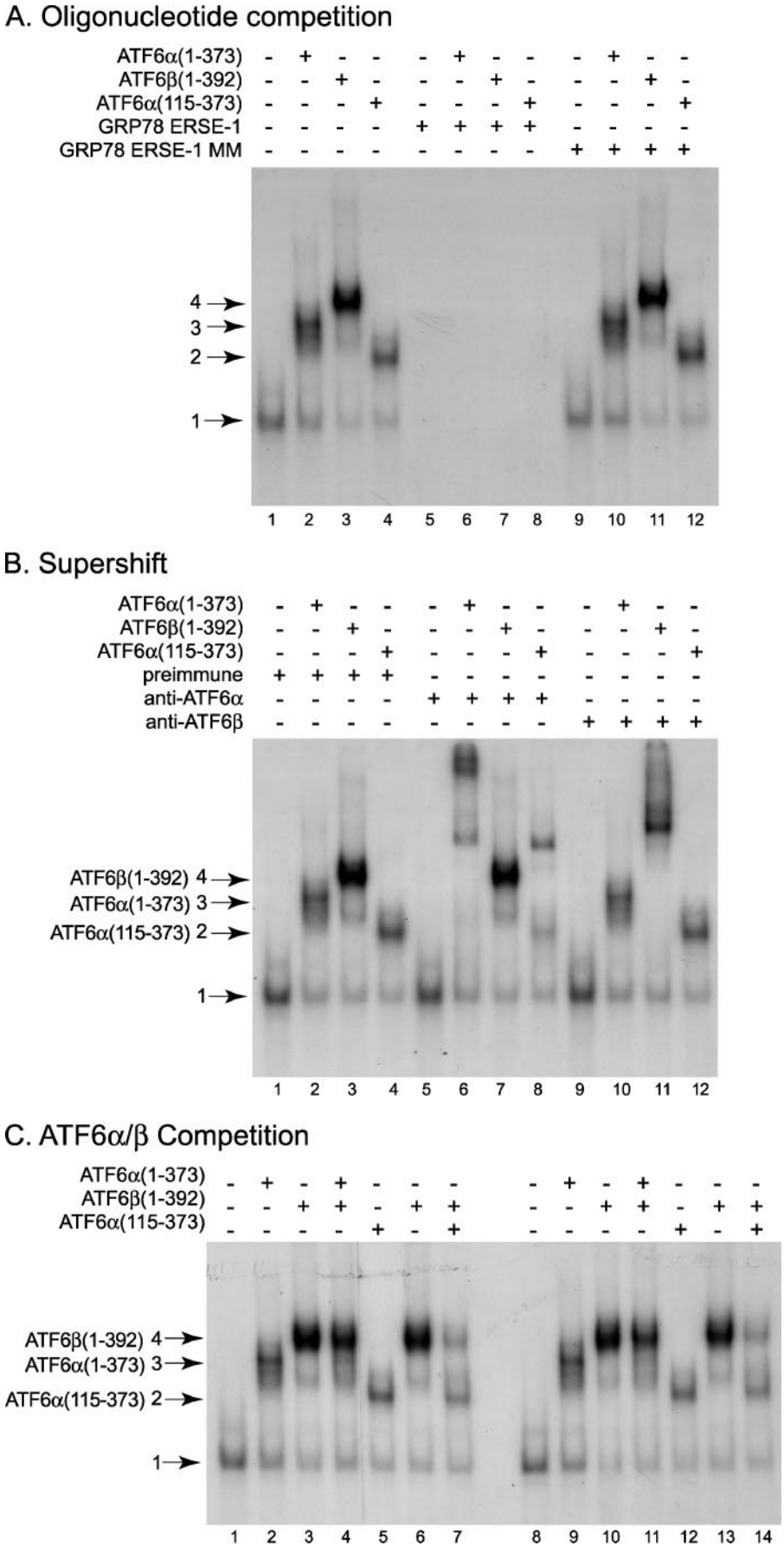

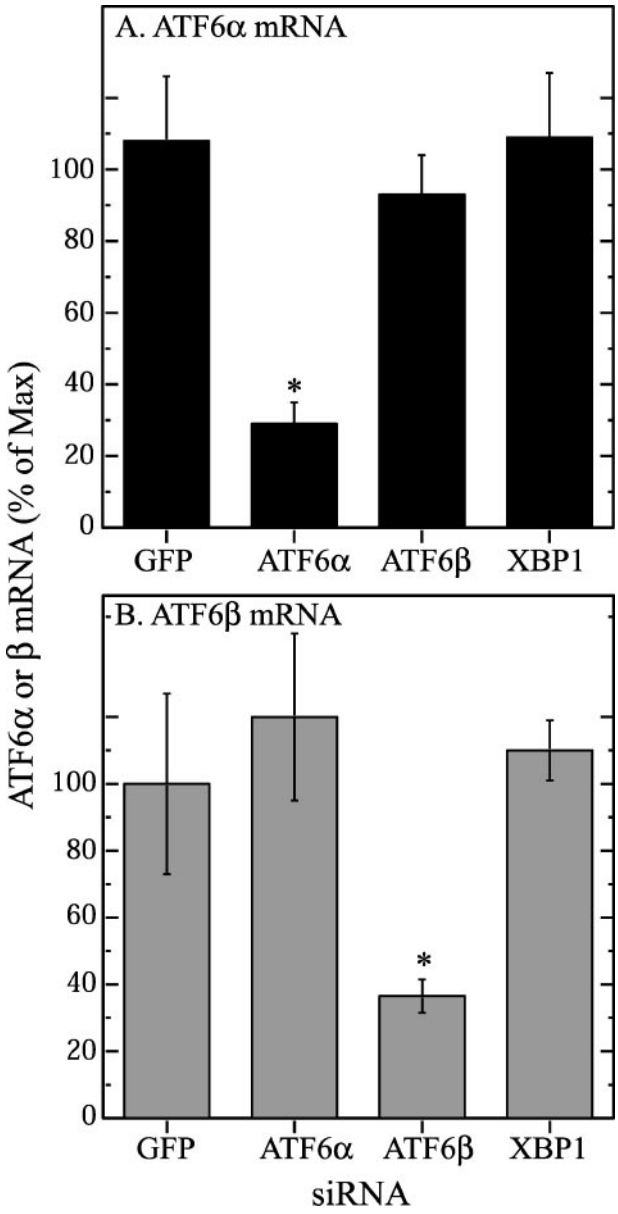

FIGURE 8. **Effect of various siRNA reagents on ATF6α or -β mRNA levels.** *A*, ATF6α mRNA: cultures were transfected with siRNA targeted against green fluorescent protein (*GFP*), ATF6α, ATF6β, or XBP1; 48 h later, cell extracts were analyzed for ATF6α mRNA by quantitative reverse transcription-PCR, as described under "Methods." Mean mRNA levels (% of maximum) ± S.E., $n = 3$ cultures are shown. *, $p < 0.05$ are different from all other values, as determined using ANOVA followed by Newman-Keuls post hoc analysis. *B*, ATF6β mRNA: cultures were transfected with siRNA and extracted as described in *A*, except ATF6β mRNA levels were assessed by quantitative reverse transcription-PCR, as described under "Methods." Mean mRNA levels (% of maximum) ± S.E., $n = 3$ cultures are shown. *, $p < 0.05$ are different from all other values, as determined using ANOVA followed by Newman-Keuls post hoc analysis. GFP-targeted siRNA was used as a control for an siRNA targeted to a non-expressed protein, and XBP1-targeted siRNA was used as a control to show that targeting a non-ATF6-related transcript did not affect the levels of ATF6α or -β mRNA.

GRP78 promoter activity by ~2- to 3-fold (Fig. 9*A*, *bars 1 versus 2* and *4 versus 5*). In contrast, knocking down endogenous ATF6β had little effect on basal GRP78 promoter activity, but it increased TM-induced GRP78 luciferase by 2-fold (Fig. 9*A*, *bars 4 versus 6*). Coordinate with these results were the findings that knockdown of ATF6α decreased TM-induced GRP78 mRNA by ~2-fold (Fig. 9*B*, *bar 4 versus 5*), whereas knockdown of ATF6β increased TM-induced GRP78 mRNA by ~1.5-fold (Fig. 9*B*, *bar 6*). Because many ERSR genes, including GRP78, encode proteins that foster protection, we examined the effects of knocking down endogenous ATF6α or -β on HeLa cell viability. We found that, although 32 h of TM treatment conferred no change in viability in cells treated with control siRNA (Fig. 9*C*; *bars 1 versus 4*), knockdown of ATF6α significantly decreased viability with or without TM (Fig. 9*C*; *bars 1 versus 2*, and *4 versus 5*), although knockdown of ATF6β significantly increased viability with or without TM (Fig. 9*C*; *bars 1 versus 3* and *4 versus 6*). These findings indicate that the isoform-specific characteristics of ATF6α and -β can influence TM-stimulated GRP78 expression, as well as viability of HeLa cells in ways that are consistent with the protective aspects of N-ATF6α and the putative abilities of N-ATF6β to serve as an endogenous repressor of ATF6α. Moreover, because knocking down ATF6α or β altered viability-TM, it is apparent that even in the absence of TM-mediated ER stress, ERSR genes, such as GRP78, must contribute to cell viability.

DISCUSSION

In this study we examined the structural features underlying the isoform-specific characteristics of ATF6α and -β, the coordination and mechanism of ATF6α transcriptional activation and rapid degradation, and whether the relative levels of ATF6α and -β affect their binding to ERSEs and regulate ERSR gene induction and cell viability. Our findings showed that there is structural information spanning most of the N-terminal 300 aa of ATF6α and -β that is required for isoform-specific characteristics. We also found that the rapid degradation of ATF6α is coordinate with its engagement in an active transcription complex, the latter of which can evidently be modulated by ATF6β. Lastly, we determined the ratio of ATF6α and -β that modulates ERSR gene induction, as well as cell viability, in a manner consistent with the hypothesis that ATF6α is a strong but labile transcriptional activator, whereas ATF6β is a weak, stable transcriptional activator.

In addition to transcriptional activity and the rate of degradation, the timing of ATF6α and -β activation following ER stress is likely to be another important, albeit, not thor-

FIGURE 7. **EMSAs examining the competition of ATF6α and ATF6β for binding to the GRP78 ERSE.** *A*, oligonucleotide competition: EMSA analysis was carried out as described under "Methods." Recombinant ATF6α-(1–373), ATF6α-(115–373) or -β-(1–392), used in the analyses shown in *lanes 2–4*, *6–8*, and *10–12*, respectively, were prepared by *in vitro* transcription/translation and then added to HeLa cell nuclear extracts. The ^{32}P-labeled GRP78 ERSE-1 probe was added to initiate the binding reactions. Complex 1 has been shown to be to the direct binding of nuclear extract-derived proteins, *e.g.* NF-Y, YY1, etc., to the ERSE. Under these experimental conditions, the binding of these accessory proteins is required before ATF6 will bind. Unlabeled double-stranded oligonucleotides representing the native GRP78 EMSA-1, or the mutated GRP78 EMSA-1 (*MM*) were added to *lanes 5–8* and *9–12*, respectively. *B*, supershift: EMSA was carried out as described in *A*, *lanes 1–4*, except for the addition of either pre-immune, ATF6α, or ATF6β antisera to *lanes 1–4*, *5–8*, or *9–12*, respectively. *C*, ATF6α/β competition: EMSA was carried out as described in *A*, except for the addition of recombinant ATF6α and -β together with nuclear extracts in *lanes 4*, *7*, *11*, and *14*. *Lanes 8–14* are replicate incubations of those shown in *lanes 1–7*.

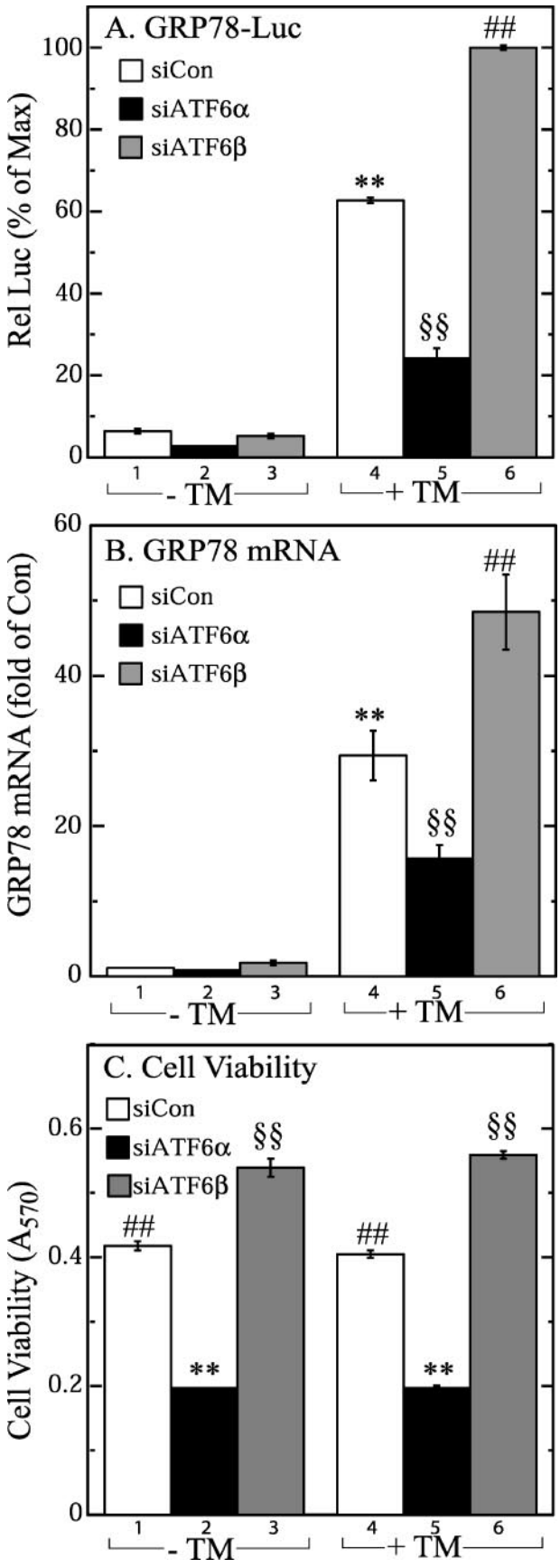

FIGURE 9. **Effect of ATF6α or -β siRNA on GRP78 induction and cell viability.** *A*, GRP78-Luciferase: HeLa cells were transfected with GRP78-luciferase, CMV-β-galactosidase, and the siRNA shown, and then treated with or without tunicamycin (2 μg/ml) for 32 h. Cell extracts were then analyzed for reporter enzyme activities, as described under "Methods." Values shown are mean ± S.E. ($n = 3$). All-TM values are in one group, whereas **, ##, and §§ = $p < 0.01$ are different from all other values, as determined using ANOVA followed by Newman-Keuls post hoc analysis. *B*, GRP78 mRNA: HeLa cells were treated as in *A*, except they were not transfected with reporter enzymes, and RNA was extracted. Values shown are mean ± S.E. ($n = 3$). All - TM are in one group, while **, ##, and §§ = $p < 0.01$ are different from all other values, as determined using ANOVA followed by Newman-Keuls post hoc analysis. *C*, Viability: Hela cells were treated as in *B*, except after siRNA transfection, they were transferred into 96-well plates, treated with or without TM (2 μg/ml) in 3 mM 2-doxyglucose (2-DG) for 32 h, then cell viability was determined, as described under "Methods." Values shown are mean ± S.E. ($n = 3$). **, ##, and §§ = $p < 0.01$ are different from all other values, as determined using ANOVA followed by Newman-Keuls post hoc analysis.

oughly studied isoform-specific characteristic. Although it is well known that both ATF6 isoforms are cleaved upon ER stress, to our knowledge, only one study showed that, depending on the stress, activation of ATF6α can occur earlier than that of ATF6β (19). Combined with their isoform-specific characteristics, sequential activation of the ATF6 isoforms (Fig. 10*A*) is consistent with the possibility that their relative levels could change as a function of time after ER stress, such that there is an initial, strong activation of ATF6-mediated ERSR gene induction, followed by modulation toward weak activation (Fig. 10*B*). One potential mechanism by which ATF6α and -β could regulate the strength of ER stress involves how these isoforms bind to ERSR genes. ATF6α and -β bind to ERSEs, and possibly other elements, as dimers, which, interact with the C subunit of the NF-Y A, B, and C trimer (19), as well as with other proteins, *e.g.* SRF (5), TFII-I (12), and perhaps YY1 (13). Together, these proteins evidently facilitate ERSR gene induction. Thus, it is conceivable that, as a result of isoform-specific rates of generation and degradation, the relative levels of ATF6α and -β in transcriptional complexes change during progression of the ERSR and that, as a result of differences in their transcriptional activities, ERSR gene induction is finely tuned, as shown in Fig. 10*C*. The results of the gel shift experiments in this study showed that ATF6α and -β can compete with each other for binding to the GRP78 ERSE (Fig. 7*C*), which lends further support to this hypothesis.

The mechanism governing the rate of degradation of ATF6 during transcription is not known. However, a great deal is known about the coupling of transcriptional activation and rapid degradation of other labile transcription factors, *e.g.* c-Myc, Gal4, VP16, SMAD2, STAT, and Hac1p (29). In those cases, the most active transcription factors are also very susceptible to ubiquitination and proteasome-mediated degradation, both of which evidently take place during engagement in transcription (15, 30). This "unstable when active" phenomenon is thought to allow tight control over transcription by ensuring that the activation of target genes is linked to the ongoing synthesis of the transcriptional regulator (30). Accordingly, such transcription factors are usually potent target gene activators, which must effect their function in a transient manner, although, rapid degradation of transcription factors has been linked to modulation as well as augmentation of activity (31, 32). Because ubiquitin-ligase/proteasome machinery exists in the nucleus and is

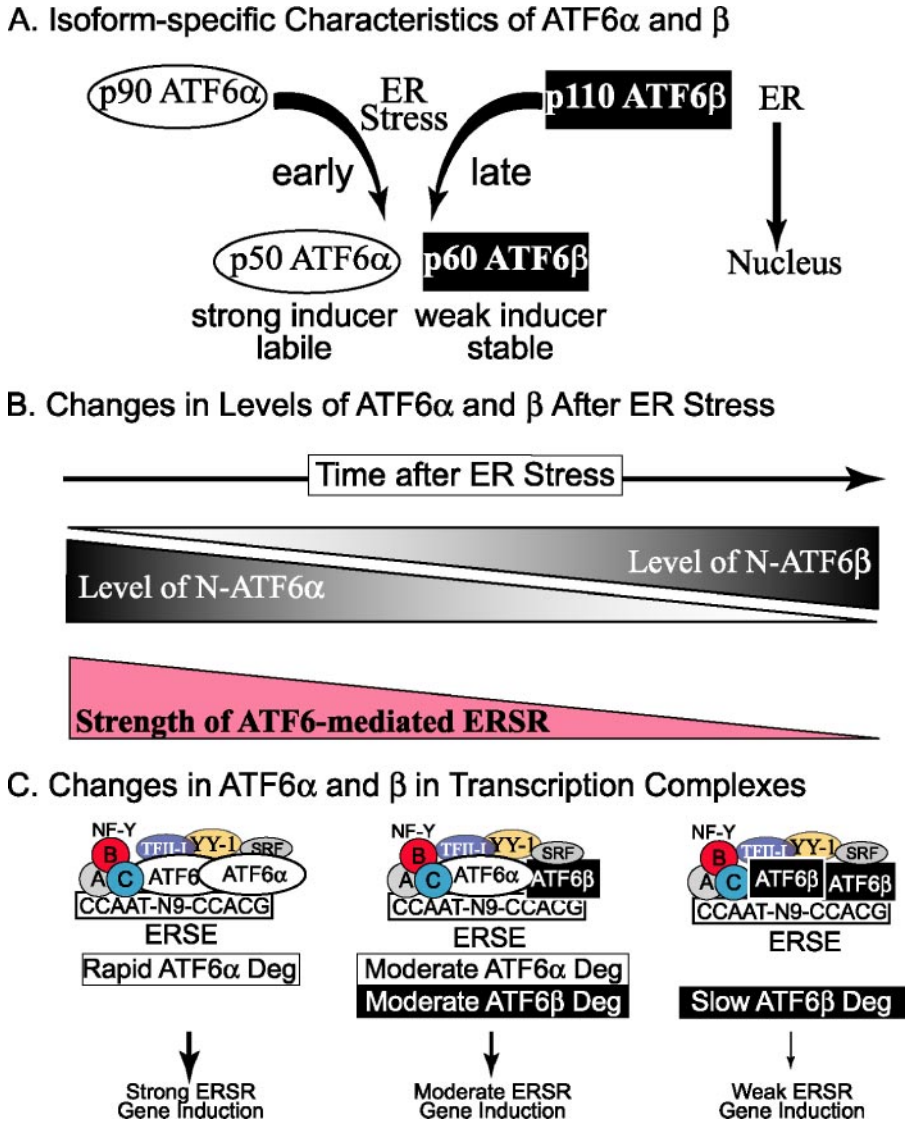

FIGURE 10. **Hypothetical roles for the isoform-specific characteristics of ATF6α and -β in modulating the strength of ATF6-mediated gene induction during the ERSR.** *A*, isoform-specific characteristics of ATF6α and -β: the *diagram* shows the approximate sizes of each form of ATF6 before and after ER stress, as well as the strength and stability of each form after ER stress. *Early* and *late* refer to hypothetical isoform-specific times of maturation during ER stress. *B*, changes in levels of ATF6α and -β after ER stress: shown at the *top* is a timeline of ER stress. The areas in the *gray triangles* represent hypothetical, reciprocal changes in the levels of ATF6α and -β that could take place as a function of time after ER stress. The *red triangle* depicts possible changes in the strength of the ATF6 branch of the ER stress response as a function of time after ER stress, and differences in the relative levels of N-ATF6α and -β. *C*, changes in ATF6α and -β in transcriptional complexes: the three model transcription complexes depict possible differences in ATF6 isoform composition and ERSR gene expression, as well as ATF6α and -β degradation rates. ATF6 is known to combine with other proteins, *e.g.* NF-Y trimers, TFII-I, YY-1, and SRF, in transcription complexes on some ERSR genes. Changes in the relative levels of ATF6α and -β may coordinate with changes in the rates of ERSR gene expression but also the rates of degradation of each ATF6 isoform.

intimately associated with active transcription complexes, it has been proposed that proteasome-mediated degradation of certain transcription factors occurs as they become engaged in transcriptional activation and may actually require polymerase II. The polymerase II requirement might contribute to distinguishing the half-lives of N-ATF6α and -β; presumably, because N-ATF6β is a poor transcriptional activator, it does not engage in a transcriptional complex that efficiently recruits active polymerase II. It was recently shown in yeast that the ER stress-activated transcription factor, Hac1p, which is homologous to another mammalian ER stress-activated transcription factor, XBP1, is degraded rapidly upon ER stress; moreover, Hac1p degradation requires nuclear localization and was impaired by Hac1p mutations that forced its nuclear exclusion (33). These findings suggest that, like ATF6α, transcriptional induction by Hac1p in yeast, and perhaps by XBP1 in mammalian cells, is engineered to be rapid and transient. The sequence responsible for Hac1p rapid degradation was localized using PESTFind (34), to a PEST motif, *i.e.* a stretch of the protein that is enriched in proline, glutamine, serine and threonine. This motif has been found in numerous other rapidly degraded proteins that are degraded in a conditional manner (35). Using PESTFind, we identified a potential PEST sequence in N-ATF6α that exhibits a similar PESTFind score as that found in Hac1p, and resides in a region, suggested by the domain-swap mutations carried out in this study, to be critical for transcriptional induction and rapid degradation of ATF6α. Thus, it will be of interest to examine whether this potential PEST sequence contributes to the rapid degradation of N-ATF6α upon transcriptional engagement.

ERSR gene expression by ATF6 is apparently regulated, in part, by the isoform-specific characteristics of ATF6α and -β. The results presented in this study suggest that it is possible that these isoform-specific characteristics contribute to ATF6-mediated gene induction in subtle ways that fine-tune this aspect of the ERSR. Future studies examining the impact of ATF6α and -β in various cells and tissues subjected to ER stress will be required to fully appreciate the roles of these ATF6 isoforms in this complex process.

REFERENCES

1. Spear, E., and Ng, D. T. (2001) *Traffic* **2,** 515–523
2. Liu, C. Y., and Kaufman, R. J. (2003) *J. Cell Sci.* **116,** 1861–1862
3. Ron, D. (2002) *J. Clin. Invest.* **110,** 1383–1388
4. Kaufman, R. J. (2002) *J. Clin. Invest.* **110,** 1389–1398
5. Zhu, C., Johansen, F. E., and Prywes, R. (1997) *Mol. Cell. Biol.* **17,** 4957–4966
6. Yoshida, H., Haze, K., Yanagi, H., Yura, T., and Mori, K. (1998) *J. Biol.*

Chem. **273,** 33741–33749
7. Ye, J., Rawson, R. B., Komuro, R., Chen, X., Dave, U. P., Prywes, R., Brown, M. S., and Goldstein, J. L. (2000) *Mol. Cell* **6,** 1355–1364
8. Haze, K., Yoshida, H., Yanagi, H., Yura, T., and Mori, K. (1999) *Mol. Biol. Cell* **10,** 3787–3799
9. Wang, Y., Shen, J., Arenzana, N., Tirasophon, W., Kaufman, R. J., and Prywes, R. (2000) *J. Biol. Chem.* **275,** 27013–27020
10. Thuerauf, D. J., Arnold, N. D., Zechner, D., Hanford, D. S., DeMartin, K. M., McDonough, P. M., Prywes, R., and Glembotski, C. C. (1998) *J. Biol. Chem.* **273,** 20636–20643
11. Roy, B., and Lee, A. S. (1999) *Nucleic Acids Res.* **27,** 1437–1443
12. Parker, R., Phan, T., Baumeister, P., Roy, B., Cheriyath, V., Roy, A. L., and Lee, A. S. (2001) *Mol. Cell. Biol.* **21,** 3220–3233
13. Li, M., Baumeister, P., Roy, B., Phan, T., Foti, D., Luo, S., and Lee, A. S. (2000) *Mol. Cell. Biol.* **20,** 5096–5106
14. Thuerauf, D. J., Morrison, L. E., Hoover, H., and Glembotski, C. C. (2002) *J. Biol. Chem.* **277,** 20734–20739
15. Salghetti, S. E., Muratani, M., Wijnen, H., Futcher, B., and Tansey, W. P. (2000) *Proc. Natl. Acad. Sci. U. S. A.* **97,** 3118–3123
16. Desterro, J. M., Rodriguez, M. S., and Hay, R. T. (2000) *Cell Mol. Life Sci.* **57,** 1207–1219
17. Tanaka, M. (1996) *Proc. Natl. Acad. Sci. U. S. A.* **93,** 4311–4315
18. Molinari, E., Gilman, M., and Natesan, S. (1999) *EMBO J.* **18,** 6439–6447
19. Haze, K., Okada, T., Yoshida, H., Yanagi, H., Yura, T., Negishi, M., and Mori, K. (2001) *Biochem. J.* **355,** 19–28
20. Yoshida, H., Okada, T., Haze, K., Yanagi, H., Yura, T., Negishi, M., and Mori, K. (2001) *Mol. Cell. Biol.* **21,** 1239–1248
21. Regier, J. L., Shen, F., and Triezenberg, S. J. (1993) *Proc. Natl. Acad. Sci. U. S. A.* **90,** 883–887
22. Thuerauf, D. J., Morrison, L., and Glembotski, C. C. (2004) *J. Biol. Chem.* **279,** 21078–21084
23. Thuerauf, D. J., Marcinko, M., Gude, N., Rubio, M., Sussman, M. A., and Glembotski, C. C. (2006) *Circ. Res.* **99,** 275–282
24. Martindale, J. J., Fernandez, R., Thuerauf, D., Whittaker, R., Gude, N., Sussman, M. A., and Glembotski, C. C. (2006) *Circ. Res.* **98,** 1186–1193
25. Yoshida, H., Okada, T., Haze, K., Yanagi, H., Yura, T., Negishi, M., and Mori, K. (2000) *Mol. Cell. Biol.* **20,** 6755–6767
26. Corton, J. C., Moreno, E., and Johnston, S. A. (1998) *J. Biol. Chem.* **273,** 13776–13780
27. Littlewood, T. D., Hancock, D. C., Danielian, P. S., Parker, M. G., and Evan, G. I. (1995) *Nucleic Acids Res.* **23,** 1686–1690
28. Yoshida, H., Oku, M., Suzuki, M., and Mori, K. (2006) *J. Cell Biol.* **172,** 565–575
29. Collins, G. A., and Tansey, W. P. (2006) *Curr. Opin. Genet. Dev.* **16,** 197–202
30. Muratani, M., and Tansey, W. P. (2003) *Nat. Rev. Mol. Cell Biol.* **4,** 192–201
31. Lipford, J. R., and Deshaies, R. J. (2003) *Nat. Cell Biol.* **5,** 845–850
32. Lipford, J. R., Smith, G. T., Chi, Y., and Deshaies, R. J. (2005) *Nature* **438,** 113–116
33. Pal, B., Chan, N. C., Helfenbaum, L., Tan, K., Tansey, W. P., and Gething, M. J. (2007) *Mol. Biol. Cell* **18,** 426–440
34. Rogers, S., Wells, R., and Rechsteiner, M. (1986) *Science* **234,** 364–368
35. Rechsteiner, M., and Rogers, S. W. (1996) *Trends Biochem. Sci.* **21,** 267–271
36. Picard, D. (1993) *Trends Cell Biol.* **3,** 278–280